The effects of dolomitization on petrophysical properties and fracture distribution within rift-related carbonates (Hammam Faraun Fault Block, Suez Rift, Egypt)

DOI:
10.1016/j.jsg.2017.06.005

Document Version
Accepted author manuscript

The effects of dolomitization on petrophysical properties and fracture distribution within rift-related carbonates (Hammam Faraun Fault Block, Suez Rift, Egypt)

Korneva I.[1], Bastesen E.[2], Corlett H.[3], Eker A.[4], Hirani J.[5], Hollis C.[5], Gawthorpe R.L.[1], Rotevatn A.[1], Taylor R.[5]

[1]Department of Earth Science, University of Bergen, Norway
Allégaten 41, 5007 Bergen, Norway
irina.korneva@uib.no*
mobile: +47 45396043
rob.gawthrope@uib.no
atle.rotevatn@uib.no
[2]Uni Research CIPR, Geosciences, Bergen, Norway
Nygårdsgaten 112, 5008 Bergen, Norway
Eivind.bastesen@uib.no
[3] Alberta Geological Survey, Edmonton, AB, Canada
4999 98 Ave NW, Edmonton, AB T6B 2X3, Canada
hilary.corlett@aer.ca
[4] Statoil, Norway
Forusbeen 50, 4035 Stavanger, Norway
anjaeker@hotmail.com
[5] School of Earth and Environmental Sciences, University of Manchester
Oxford Road, Manchester, M13 9PL
Jesal.hirani@hotmail.com
Cathy.Hollis@manchester.ac.uk
Rochelle.Taylor@manchester.ac.uk

Keywords: limestones; dolostones; textural and petrophysical properties; fracture spacing

ABSTRACT

Petrographic and petrophysical data from different limestone lithofacies (skeletal packstones, matrix-supported conglomerates and foraminiferal grainstones) and their dolomitized equivalents within a slope carbonate succession (Eocene Thebes Formation) of Hammam Faraun Fault Block (Suez Rift, Egypt) have been analyzed in order to link fracture distribution with mechanical and textural properties of these rocks. Two phases of dolomitization resulted in facies-selective stratabound dolostones extending up to two and a half kilometers from the Hammam Faraun Fault, and massive

dolostones in the vicinity of the fault (100 metres). Stratabound dolostones are characterized by up to 8 times lower porosity and 6 times higher frequency of fractures compared to the host limestones. Precursor lithofacies type has no significant effect on fracture frequency in the stratabound dolostones. At a distance of 100 metres from the fault, massive dolostones are present which have 0.5 times porosity of precursor limestones, and lithofacies type exerts a stronger control on fracture frequency than the presence of dolomitization (undolomitized vs. dolomitized). Massive dolomitization corresponds to increased fracture intensity in conglomerates and grainstones but decreased fracture intensity in packstones. This corresponds to a decrease of grain/crystal size in conglomerates and grainstones and its increase in packstones after massive dolomitization.

Since fractures may contribute significantly to the flow properties of a carbonate rock, the work presented herein has significant applicability to hydrocarbon exploration and production from limestone and dolostone reservoirs, particularly where matrix porosities are low.

1. INTRODUCTION

Dolomitization in carbonate reservoirs affects the distribution of petrophysical rock properties and may enhance or degrade porosity (Lucia and Major, 1994; Purser et al., 1994; Lucia, 2004). Furthermore, the different mechanical and textural characteristics of dolostones with respect to limestone may result in a change of pore shape and size, and fracture intensity that causes major variability in permeability (Rustichelli et al., 2015; Giorgioni et al., 2016). Nevertheless, the specifics of how dolomitization affects petrophysical properties and fracture distribution within carbonate rocks are largely uncertain (Purser et al., 1994; Lucia, 2004; Laubach et al. 2009; Ehrenberg et al., 2012; Nelson, 2015).

Textural and petrophysical properties of dolostones are likely to be affected by many parameters, including dolomitization rate, temperature, the concentration of Mg in dolomitizing fluids, depth, structural setting and precursor permeability, the latter of which itself is a function of facies type and prior diagenetic modification (Machel, 2004). Some studies of dolostones have proposed that they had higher porosity than limestone as a result of "mole-per-mole" replacement (Blatt et al., 1972; Amthor et al., 1993, 1994). Other authors have demonstrated that limestones lose porosity more rapidly than dolostones through compaction and cementation (Schmoker and Halley, 1982; Lucia, 2004). However, lower porosity in dolostones with respect to their precursor limestone is seen (Schmoker et al., 1985; Saller, 2013), particularly in dolostones buried to less than 1-2 km (Schmoker and Halley, 1982; Halley and Schmoker, 1983; Allan and Wiggins, 1993; Sun, 1995; Machel, 2004). In particular, during dolomitization, progressive cementation of pore space with dolomite cement ("overdolomitization") can lead to a significant reduction of porosity (Saller and Henderson, 2001; Lucia, 2002, 2004; Gale et al., 2010).

Many studies have documented more intense fracturing of dolostones than limestone (Schmoker et al., 1985; Nelson, 2001; Ortega & Marrett, 2001; Gale et al., 2004); yet, some studies show the opposite (Beliveau et al., 1993, Rustichelli et al., 2015). Dati et al. (2013) proposed that limestone and dolostone with the same grain/crystal size display the same fracture spacing, and therefore, that *rock texture* (crystal/grain size) (rock lithology) is a more important factor than mineralogy in regulating the fracture pattern. The importance of crystal size on fracturing was highlighted by Flugel et al. (2010) and Rustichelli et al. (2015), who documented that coarse-crystalline dolostones are less densely fractured than fine-crystalline dolostones. However, the influence of different precursor limestone lithologies on the textural and petrophysical properties of dolostones, and how that in turn affects fracture frequency in limestone vs. dolomitized rock pairs (e.g. dolomitized grainstone vs undolomitized grainstone, dolomitized packstone vs. undolomitized packstone) is still uncertain.

In this paper, we investigate the relationship between dolomitization, petrophysical properties fracturing, and, most importantly, how these relate to the initial textural properties of the precursor limestones. The study area, the Hammam Faraun Fault Block (HFFB), Gulf Suez is a well-exposed location, where the mechanical control on fracture frequency in different limestone lithofacies and their dolomitized equivalents can be studied. Three different limestone lithofacies of Eocene Thebes Formation are exposed in the HFFB: (i) matrix-supported conglomerates, interpreted as debris flows, (ii) skeletal grainstones, interpreted as turbidites and (iii) skeletal packstones, interpreted as slope deposits (Hirani, 2014). The primary objective of this work is to assess the mechanical control on fracture distribution in light of petrophysical and textural variability in the studied limestone-dolostone succession. This objective is achieved by answering the following specific questions:

1. How does fracture distribution vary between different limestone lithofacies (i.e. packstone, grainstone, and conglomerate), and which textural and petrophysical properties control fracture distribution?
2. How does fracture distribution vary between dolostones with different precursor limestone lithofacies, and which textural and petrophysical factors exert control on fracture distribution?
3. How does fracture distribution vary between limestone-dolostone pairs of equivalent lithofacies, and which textural and petrophysical factors control fracture distribution?

By answering these questions we may increase our understanding of how dolomitization induced changes in the mechanical and petrophysical properties of carbonate rocks may affect fracture distribution. This, in turn, has implications for predicting the distribution of porosity and permeability in fractured limestone-dolostone successions, which form important reservoirs for hydrocarbons and other fluids worldwide.

2. GEOLOGICAL SETTING

The Suez Rift is about 300 km long and 80 km wide, representing the aborted NW–SE-trending extension of the Red Sea rift system. The main rift phase occurred in the late Oligocene to Miocene (c. 24-15.5 Ma (e.g. Patton et al. 1994; Sharp et al., 2000; Khalil & McClay 2001; Bosworth et al. 2005) before the initiation of the Dead Sea–Aqaba transform (Cochran 1983). GPS-derived velocity and crustal strain field analysis suggest that the Gulf of Suez is still actively extending (El-Fiky, 2005).

The Suez rift displays classical rift geometries including numerous half-grabens and rotated fault blocks that are bounded by extensional faults with kilometres of displacement (Moustafa and Abdeen 1992; Sharp et al., 2000; Khalil and McClay 2001; Fig. 1). The Hammam Faraun Fault Block (HFFB) is located on the western side of the Sinai Peninsula and bounded by the Thal fault to the east and the Hammam Faraun Fault (HFF) to the west (Moustafa & Abdeen, 1992; Sharp et al., 2000; Fig. 1). The HFF is a crustal scale NW-SE striking fault with approximately five kilometres of displacement (Gawthorpe et al., 2003; Jackson et al., 2006), controlling the position of present day shoreline. The study area is located in the northwestern corner of the HFFB, in the footwall of the HFF and up to 2.5 kilometres away from the fault itself (Fig. 1A-B). The HFFB is affected by a range of intra-block faults with lesser throws (generally up to a few 100 meters) that were active at the rift initiation stage (24 Ma onwards), before displacement localized onto the HFF during the rift climax 6-7 My later (Gawthorpe et al. 2003). Seismic reflection data indicate that the HFF accumulated a significant amount of displacement after the main Oligo-Miocene rift event (Gawthorpe et al., 2003, Jackson & Rotevatn, 2013). Uplift of Quaternary coral terraces in the footwall up to 10-15 metres above present sea-level support Late Quaternary activity on the HFF (Gawthorpe et al. 2003).

The stratigraphy of the Suez Rift can be subdivided into pre-rift (Cambrian to Eocene) and syn-rift (Oligocene-Quaternary) (Sharp et al. 2000; Moustafa 2004). The pre-rift Palaeozoic to Lower Cretaceous Nubian sandstone was deposited regionally throughout Northern Africa and the Middle East and unconformably overlies Precambrian igneous and metamorphic basement rocks (Moustafa and Abdeen 1992; Bosworth 1995; Moustafa 1996; Gupta et al. 1999). Nubian sandstones are overlain by Upper Cretaceous to Oligocene mixed marine siliciclastics and carbonate deposits (Moustafa and Abdeen, 1992; Sharp et al., 2000; Fig. 1C). The Thebes Formation (the unit of interest in the present study) is a part of a late pre-rift Palaeocene to Eocene carbonate succession (Abul-Nasr and Thunell, 1987; Moustafa and Abdeen, 1992; Spence and Finch, 2014). In this study area, the Thebes Formation comprises skeletal pack- to wackestones intercalated with conglomerates and skeletal grainstones (see results sections; Corlett et al., in prep). Syn-rift deposits unconformably overly pre-rift deposits and are composed of marginal to deep marine siliciclastics with local carbonate development (Jackson et al., 2005).

Insert Figure 1

The lower Thebes Formation includes remobilized slope deposits comprised of three main lithofacies: (i) matrix-supported conglomeratic debris flows and (ii) turbiditic pack-grainstones embedded within (iii) slope packstone deposits (Hirani, 2014); from here on we will refer to these simply as conglomerates, grainstones and packstones. The Thebes Formation is partially dolomitized within the footwall of the HFF and includes two types of dolostone bodies formed during two phases of dolomitization (Fig. 2). Firstly, stratabound dolostones were formed during the rift initiation stage (~26 Ma; Hirani, 2014; Hollis et al., 2017) and, secondly, massive dolostone pods were formed during the rift climax stage (24-17 Ma; Hirani, 2014; Hollis et al., 2017).

Two massive dolostone pods are located in the vicinity of the HFF; these are ~80 m thick and up to 500 m wide (Hollis et al., 2017). Massive dolostones are bounded by the shale-dominated Esna Formation at the base (Fig. 1C), and by fine-grained sediments within the lower Thebes Fm. at the top. Laterally, these massive dolostone pods are structurally separated from adjacent limestones by sub-vertical fracture corridors. These fracture corridors form 1-5 m wide zones, and there is no shear displacement associated with them. The north massive dolomite body is bounded structurally to the east by a N-S trending, steeply east-dipping (~80°) fracture corridor. The southern massive dolomite body is bounded structurally to the northeast by a NW-SE trending, steeply northeast-dipping (~70°) fracture corridor.

Stratabound dolostones extend from the fault up to 2.5 km into the HFFB, ranging in length from 5 to 300 m and in thickness from 25 cm to 15 m. The stratabound dolostones are restricted to grainstone and conglomerate beds.

Insert Figure 2

3. METHODOLOGY

Spatial and dimensional attributes of fractures were collected within limestones and dolostones by means of scanlines acquired in the vicinity and 1.5-2 kilometres away from the HFF (Wadi Wasit and Y-shaped Wadi areas; Fig. 1B). More than 50 scanlines were made within the three different lithofacies (packstone, grainstone and conglomerate) and their dolomitized equivalents (stratabound dolostones far away from the fault, and massive dolostones in the vicinity of the fault). Data recorded included fracture type, orientations, intensity (number of fractures per meter), fracture termination (stratabound or non-stratabound fractures). Fracture intensity was converted into spacing, which was subsequently normalized by bed thickness for both stratabound and non-stratabound fractures, for each scanline. This was done in order to eliminate an influence of bed thickness and to understand the mechanical control on fracture spacing. The coefficient of variation (standard deviation divided mean value) was calculated for fracture spacing for each lithology. Each bed where scan lines were made was also sampled for petrographic and petrophysical analysis.

Textural, petrographic and petrophysical analysis of thin sections were focused on composition, porosity, pore size and grain size. Point counting using PETROG © software was used to quantify the textural characteristics of the studied rocks with 300 points per thin section (Flugel, 2010). The percentage of clasts, matrix, pores and authigenic minerals for each limestone lithofacies was calculated, as well as the volume of replacing/cementing calcite/dolomite in dolostones. The pore types within the limestone and dolostone samples were classified according to Choquette and Pray (1970) and recorded within the 300 points. Grain/crystal size was measured petrographically, based on at least 70 grains per thin section.

Petrophysical measurements were undertaken on 70 samples (30 limestone and 40 dolomite samples). Cylindrical samples of 25 mm diameter and varying length (14-75 mm) were used to determine porosity and permeability. Permeability was measured using nitrogen gas that was intruded using a ResLab^{TM} DGP-200 digital gas permeameter. Porosity was determined from sample weight and grain volume that was measured by helium injection using a ResLabTM DHP-100 digital helium porosimeter. Microporosity (all pores that are less than 30 micron) was calculated by subtracting total porosity measured by image analysis, using ImageJ (Grove and Jerram, 2011) from total gas porosity measured by helium intrusion. Young's modulus was calculated from Vp, Vs, and density measured at hydrostatic pressures up to 100 MPa on rock cores.

4. TEXTURAL CHARACTERISTICS AND PETROPHYSICAL PROPERTIES

Here the three limestone lithofacies (i.e. packstone, grainstone and conglomerate) and their dolomitized equivalents related to stratabound and massive dolostones are described in terms of composition, texture, grain and pore size, pore types, and porosity. The data are arranged according to precursor limestone lithofacies, which experienced a first and second phase of dolomitization (stratabound and massive dolostones).

4.1. ***Conglomerate***

Matrix-supported conglomerates (*undolomitized;* see Table 1) range in bed thickness from 30 cm to over 20 m, and feature sharp, irregular bases and concave upper contacts. The conglomerates are characterized by poorly sorted, subangular foraminiferal packstone and grainstone clasts that are 1-50 cm in diameter, in a matrix of foraminiferal wackestone (Fig. 3A; Hirani, 2014). The matrix constitutes up to 24% and the amount of bioclasts is up to 64% of the rock volume in the conglomerate (Fig. 4A).

Authigenic minerals are up to 11% of the rock volume and are dominated by calcite and dolomite cements. Macroporosity in the conglomerates is mainly mouldic (~27% of the pore volume), with minor amounts of intergranular, intragranular and fracture porosity (Fig. 4D). Moreover, there is abundant mouldic porosity after clasts, which are too big to be captured by petrographic analysis (cm-sized).

The matrix displays micro- and intergranular porosity and is generally more porous than the clasts. The principal pore types in the clasts are mouldic and vuggy. The average total porosity is about 9% and pore size ranges between 65 and 85 µm (average = 73 µm) (Fig. 5B, C). The average Young's modulus value is 58 GPa.

Dolomitized conglomerates within the massive dolostone bodies (Table 1) show locally preserved fabric with distinguishable clasts and matrix (Fig. 6A, B). They exhibit both non-planar and planar-s textures (*sensu* Sibley and Gregg, 1987) with cloudy cores and clear rims. The massive dolostones consist of 72% replacive dolomite, with up to 12% dolomite and rare calcite cement (Fig. 4B, 6B). The average Young's modulus value is 78 GPa. Crystal size of these dolostones averages 108 µm typically between 90 and 120 µm (Fig. 5A). The porosity is around 6% with a wide range of values between 3 and 10% (Fig. 5C). The average diameter of the pores is 60 µm (50 - 71µm; Fig. 5B). Pore types are mostly intercrystalline, vuggy and mouldic with minor micro, intracrystalline and fracture porosity (Fig. 4E).

Insert Table 1

Insert Figure 3

Dolomitized conglomerates within the stratabound dolostone bodies (Table 1) are characterized by non-planar and planar-s textures with cloudy cores and clear rims. They typically have about 60%

replacive dolomite, about 20% replacive calcite (dedolomite) and up to 7% calcite cement (Fig. 4C). The average Young's modulus value is 80 GPa. Crystal size averages 80 µm (Fig. 5A). Total porosity varies between 1 and 7% with the average value around 4% (Fig. 5C). Porosity calculated by image analysis is 10% higher than the total porosity. Pore diameter varies between 50 and 70 µm (average pore size 60 µm) (Fig. 5B). Based on petrographic observations, the main pore types are intercrystalline, vuggy and mouldic (Fig. 4F).

Insert Figure 4

4.2. Grainstone

Grainstones (*undolomitized;* see Table 1) in the Lower Thebes Formation are present in beds which are 0.5-10 meters thick. Individual beds have a sharp, irregular basal contact and sharp, flat upper contacts, are well-sorted and composed of benthic foraminifera, echinoid fragments, bryozoan fragments, serpulid worm tubes, dasyclads, and rare planktonic foraminifera (Hirani, 2014). The grainstones are composed of 64% grains and up to 25% matrix (Fig. 4A). The average Young's modulus value is 56 GPa. Grain size ranges between 150 µm and 170 µm (Fig. 5A) and total porosity is approximately 12%, composed of mainly intergranular and micro pores (Fig. 5C, 4D). Vuggy and mouldic pores are rare. Pore size ranges from 55 to 93 µm with an average of 77 µm (Fig. 5B).

Insert Figure 5

Dolomitized grainstones within the massive dolostone bodies (Table 1) locally display fabric preservation, with precursor bioclasts replaced by dolomite (Fig. 6D). This facies is differentiated from dolomitized conglomeratic facies in outcrop by an absence of cm-scale mouldic and vuggy pores, and abundant biomoulds, after *Nummulites*. In thin section, non-planar and planar-s textures have cloudy cores and clear rims. The rocks have up to 92% replacive dolomite and no calcite (Fig. 4B). The average Young's modulus value is 75 GPa. The average crystal size is 81 µm (69 and 96 µm; Fig. 5A).

The average porosity is 7% (5 to 9%) and comprises intercrystalline, mouldic and vuggy pores (Fig. 5C, 4E). Pore size ranges from 65 to 85 µm, with an average value of 73 µm (Fig. 5B).

Insert Figure 6

Dolomitized grainstones within the stratabound dolostone bodies (Table 1) have non-planar and planar-s textures with cloudy cores and cemented rims. This rock has by 92% replacive dolomite and rare replacive calcite (Fig. 4C). The average Young's modulus value is 84 GPa. Crystal size ranges between 95 and 122 µm with an average value of 108 µm (Fig. 5A). Average porosity is about 2% with average pore size of 52 µm (42 - 61 µm; Fig. 5C), comprising intercrystalline, intracrystalline, vuggy, mouldic, micro and fracture porosity (Fig. 4F).

4.3. ***<u>Packstone</u>***

Packstones are not affected by stratabound dolomitization, so only *undolomitized packstones* and *dolomitized packstones within massive dolostone bodies* are described below.

Packstone (*undolomitized;* Table 1) beds are dominated by foraminifera and range in thickness from 20 cm up to 6 meters with undulating upper and lower contacts. Massive beds are intercalated with packages of reddish thin beds. The average grain size is 100 µm (88 - 108 µm; Fig. 5A). The average Young's modulus value is 58 GPa. The packstones contain 52% matrix and 25% of bioclasts with 16% authigenic calcite (Fig. 4A). Porosity from image analysis is lower (6%) than total (helium) porosity (10%). Microporosity constitutes up to 43% of total porosity. Other pore types are mainly mouldic, intergranular and fracture porosity (Fig. 5C, 4D). Pore diameter ranges between 67 and 77 µm, with an average value of 72 µm (Fig. 5B).

Dolomitized packstones within the massive dolostone bodies (Table 1) preserve the macroscopic fabric of thin beds intercalated with thick, massive beds. The dolomitized packstones display non-planar and planar-s textures with cloudy cores and clear rims. Crystal size averages 139 µm, ranging from 128 up to 150 µm (Fig. 5A). Average Young's modulus is 87 GPa. The rocks have 85% replacive dolomite, up to 8% replacive calcite and rare dolomite cement (Fig. 4B). Porosity obtained by image analysis (7%) is slightly higher than total (helium) porosity (5.5%) (Fig. 4B, 5C). Pores are mainly intercrystalline (up to 52%) with up to 17% mouldic porosity (Fig. 4F). Less common pore types include intracrystalline, vuggy and fracture porosity (Fig. 6C-D). Pore diameter averages 67 µm and varies from 56 µm to 76 µm (Fig. 5B).

5. FRACTURE DISTRIBUTION

In the following section, we describe the fracture distribution in the study area, focusing on the two sub-areas in the vicinity of, and ~2km away from, the HFF (see Fig. 1B for location). The fractures we studied are non-mineralized opening-mode fractures (joints) postdated dolomitization. Apertures are uniformly small and were not systematically measured.

At a distance of 2 km from the HFF (Fig. 1B), limestones and dolostones are affected by stratabound, bed-perpendicular joints (Fig. 7A-B) which are arranged into two dominant sets: one set striking NW-SE and another one striking NNE - SSW (Fig. 8A).

In the vicinity of the Hammam Faraun Fault (100 meters from the HFF; Fig. 1B), fractures within limestones and dolostones are mostly non-strataboundand are arranged into three main sets that strike N-S, NE-SW and WNW-ESE (Fig. 8B). Stratabound joints occur but are rare, and abut against mechanical interfaces such as intra-stratal lithological contrasts and bed boundaries (e.g., reddish thin intercalated beds within packstone which remain intact after dolomitization) (Fig. 7B-D).

Fracture spacing for all the lithofacies, both in proximity to and away from the HFF, shows a positive correlation with bed thickness (Fig. 8C-D). At 2km distance from the HFF (2 km; Fig. 1B), fractures in undolomitized limestones display spacing, normalized by bed thickness, up to six times wider than stratabound dolostones (Fig. 8E). The widest fracture spacing among undolomitized limestone is in grainstones, with narrower values for conglomerates and the narrowest spacing in packstones (Fig. 8E). Among stratabound dolostones, conglomerates have a fracture spacing that is only slightly lower than that in grainstones (Fig. 8E). The coefficient of variation (Cv) is close to 0 for the fractures within each lithology (Table 2).

Insert Figure 7

Insert Table 2

Near the HFF (100 meters from the fault), an average fracture spacing (normalized to bed thickness) within the undolomitized limestones, is widest in the conglomerates, narrower in grainstones, and the narrowest in packstones (Fig. 8F). The same trend is observed for lithofacies within the massive dolostone bodies. Therefore, the narrowest fracture spacing is documented in packstone and dolomitized packstone in the vicinity of the HFF. Fracture spacing in dolomitized conglomerates and grainstones are slightly narrower than in their undolomitized equivalents, whereas dolomitized packstones have an average fracture spacing 1.5 times that of undolomitized packstone (Fig. 8F).

Insert Figure 8

6. DISCUSSION

Fracture distribution within the studied rocks is discussed in light of their lithological, textural and petrophysical properties, and the overall structural and diagenetic evolution of the study area. Firstly, factors controlling fracture distribution within undolomitized limestone lithofacies (conglomerate, grainstone and packstone) are discussed. Subsequently, we discuss how different textural and petrophysical properties of dolostones, having various precursor limestone lithofacies, affect fracture distribution within these dolostones. Finally, we discuss how fracture intensity changes in each limestone lithofacies after dolomitization, and the factors that influence this change.

6.1. Variability and controls on fracture distribution in undolomitized limestones

Three undolomitized limestone lithofacies show variable spacing of stratabound fractures at distance (2 km) from the HFF. Packstones have narrower fracture spacing than matrix-supported conglomerates, and grainstones show the widest spacing. Therefore, rocks with coarser grain sizes (grainstone) are characterized by wider fracture spacing (Fig. 5A, 9E). This is consistent with previous studies, which document that coarser-grained rocks display wider fracture spacing (Di Naccio et al., 2005; Ortega et al., 2006; Wennberg et al., 2006; Zahm et al., 2010; Ahmeed et al., 2010; Dati et al., 2011; Rustichelli et al., 2013). The influence of porosity on fracture distribution is not straightforward, since packstones have higher porosity than the conglomerates, yet the former is characterized by more frequent fractures than the latter. Therefore, the grain size is likely to have a greater impact on fracture distribution compared to the porosity of the rock (Fig. 9).

In contrast to the 2 km distant locality, conglomerates near the HFF have the most widely spaced fractures, while the fracture spacing in grainstones is lower. However, conglomerates are characterized by finer average grain size and lower porosity (Fig. 5A, C; Fig. 9). This could be related to their much less uniform texture, comprising clasts and matrix, leading to a wider range of variability in the range of grain sizes.

The pore sizes do not vary significantly between the limestone lithofacies, and are therefore not considered a major factor affecting fracture distribution in these rocks.

Insert Figure 9

6.2. Variability and controls on fracture distribution in dolostones

In both stratabound and massive dolostones, the fracture spacing reflects the trend observed in limestone lithologies (Figure 9D-E), implying a strong control by precursor texture on fracture distribution.

Within the stratabound dolostone bodies, dolomitized grainstones and conglomerates have similar values of fracture spacing (Fig. 9D). This is consistent with observations made by Giorgioni et al (2016) who documented that crystal size does not affect the intensity of stratabound fractures. However, the dolomitized conglomerate has slightly smaller crystal size and narrower fracture spacing than the dolomitized grainstone (Fig. 9A).

Within the massive dolostone bodies, there is much more variation in fracture spacing between different precursor lithofacies than that observed in the stratabound dolostones. This is consistent with Giorgioni et al. (2016), who stated that non-stratabound fracture spacing is influenced by crystal size (Fig. 9). The trend is narrower fracture spacing from dolomitized conglomerate via dolomitized grainstone to dolomitized packstone. Porosity and pore size do not vary significantly within massive dolomites, whereas crystal size differs, with the coarsest crystals occurring in dolomitized packstones, and the finest in dolomitized grainstones (Fig. 9C). Previous studies of Dati et al. (2011), Rustichelli et al. (2015) and Giorgioni et al. (2016) highlighted the control of crystal size on fracture spacing in dolostones, with more coarsely-crystalline dolostones generally being associated with greater fracture spacing than finer-crystalline dolostones. Our data partially confirms this observation: dolomitized conglomerate (massive dolomite) is characterized by coarser crystal size and wider fracture spacing than dolomitized grainstone (massive dolomite) (Fig. 10). However, dolomitized packstones, with a coarser crystal size than the other dolostones, display narrower fracture spacing compared to other dolomitized lithofacies. This may be attributed to presence of intercalated reddish thin beds within packstone that are preserved after dolomitization (Fig. 7B-C). Both stratabound and non-stratabound fractures abut against these beds; therefore, these layers appear to behave as important mechanical boundaries and reduce the effective mechanical layer thicknesses within the packstone (Table 1), resulting in narrower fracture spacing.

6.3. Textural and petrophysical controls on fracture spacing in different dolomitized lithofacies

Young's modulus describes the stiffness of a rock, and varies in this study between limestones and dolostones. Both types of dolostones (massive and stratabound) have 1.5 value of Young's modulus of the limestones. Stratabound dolostones and most of massive dolostones are more fractured than limestones, which is consistent with observations of Corbett et al. (1987), Bai et al. (2002), Lezin et al. (2009), and Rustichelli et al. (2013) that rocks with higher Young's modulus are more fractured. Stratabound dolostones have porosity that is one eighth, and fracture spacing that is one sixth their precursor limestones at the same location. This is consistent with the results of several previous studies where higher fracture frequencies were documented in dolostones compared to limestones (Nelson, 2001; Ortega & Marrett, 2001; Gale et al., 2004). Stratabound dolomitized conglomerates display half as much porosity as their limestone precursors and a similar pore size compared to undolomitized conglomerates (Fig. 9 A-B). Stratabound dolomitized grainstones exhibit 1/8 porosity and 1/2 pore size of undolomitized grainstones. The average crystal size is 80 µm for stratabound dolomitized conglomerates and 110 µm for stratabound dolomitized grainstones, which is approximately 0.5 times finer than the grain size of their precursor limestone facies. Therefore, stratabound dolomitization appears to be associated with a decrease in grain (crystal) size, decrease in porosity and increase in stiffness of the rock, leading to more pervasive fracturing.

In proximity to the HFF, porosity reduction during dolomitization is less significant (approximately one half; Fig. 9A) and there is not such a large contrast between fracture spacing in dolostones and limestones as was observed far from the fault. This could be due to the fact that fault activity associated with slip on the HFF resulted in greater deformation and higher fracture frequencies in the damage zone, which overprinted mechanical controls on fracture spacing caused by lithological variations i.e. between limestone and massive dolostone. Nevertheless, it is noteworthy that grainstones and conglomerates after dolomitization display narrower fracture spacing than their precursor limestones, whereas packstones after dolomitization are characterized by less frequent fractures. The crystal sizes of dolomitized conglomerates and grainstones are half the grain size of precursor lithofacies, whereas the crystal size of dolomitized packstone (140 µm) is 1.5 of the grain size of the precursor limestone (100 µm). In fact, dolomitized packstones have much coarser crystal sizes than dolomitized grainstones and conglomerates (Fig. 9C). The reason for this is unclear, but it could relate to a slower rate of dolomitization in packstone because of its lower permeability (Fig. 4A, D). The importance of dolostone crystal size for fracture spacing was highlighted by Dati et al. (2011) who suggested that dolostones behave similarly to limestone beds of comparable grain size, negating the change in density, and hence rigidity, associated with dolomitization. However, in our study limestones and dolostones with similar grain or crystal size do not have similar fracture spacing (Fig. 9). For example, dolomitized conglomerates (massive dolostone) and undolomitized packstones display similar grain (crystal) size, but their fracture spacing is very different (Fig. 4).

To summarise, massive dolomitization appears to be associated with porosity reduction, grain (crystal) size reduction, in the case of conglomerates and grainstones, and grain (crystal) size increase in packstones. Overall, the increase in Young's modulus indicates that dolomitization in proximity to the HFF results in stiffening of the rocks. The grain/crystal size ratio appears to present the most important parameter which affects fracture spacing in the studied dolostones, as massive dolomitization resulted in decrease of fracture spacing in conglomerates and grainstones and its increase in packstones.

7. CONCLUSIONS

Stratabound and massive dolomitization affected the petrophysical properties and fracture spacing in limestones in the Hammam Faraun Fault Block (Gulf Suez) in different ways. Stratabound dolomitization resulted in a porosity reduction to one eighth that of the precursor limestone, and an associated stiffening of the rock. This in turn led to a one sixth decrease in fracture spacing compared to precursor limestones. Stratabound dolostones after different limestone precursors do not display much variability in fracture spacing. Massive dolomitization resulted in stiffening of the rock, but a reduction of porosity of one half, compared to limestones. These dolostones reflect the trend of fracture spacing observed in precursor limestone lithofacies: the narrowest fracture spacing in packstones and the widest in conglomerates. However, the effect of massive dolostones on fracture spacing is different in various limestone lithofacies: there is an increase of fracture spacing after dolomitization in packstones and a decrease of fracture spacing after dolomitization in conglomerates and grainstones. This is consistent with the increase of grain/crystal size in packstone and its decrease in conglomerate and grainstone after dolomitization. These observations confirm that crystal size and grain/crystal size ratio are significant parameters which influence the way dolomitization affects fracture spacing; and that these parameters appear to be more important than porosity and pore size. For this reason, knowledge of the grain size and texture of precursor limestone and the crystal size of resultant dolostones are critical to predicting the rock mechanical properties of a partially dolomitized succession. These results enhance our knowledge about how dolomitization may affect fracture distribution, and, thus, a quality of limestone-dolostone reservoirs.

ACKNOWLEDGEMENTS

This project was funded via ITF project 3310PSD by BG-Group, Saudi Aramco, Statoil and Total. The lead author I. Korneva was supported by a postdoctoral scholarship from VISTA (project no. 6267) - a basic research program and collaborative partnership between the Norwegian Academy of Science and Letters and Statoil. Falcon of the Desert, Thomas Berg Kristensen, Michael Laukemann, Thomas Seers, Richard Newport and David Hodgetts are gratefully acknowledged for field support.

REFERENCES

Abul-Nasr, R.A., Thunell R.C., 1987. Eocene eustatic sea level changes, evidence from Western Sinai, Egypt. Palaeogeography, Palaeoclimatology, Palaeoecology 58(1-2), 1-9.

Ahmed Elfeel, M., Couples, G.D., Geiger, S., Ma, J., 2010. Upscaled multi-phase flow properties of fracture corridors. SPE Caspian Carbonates Technology Conference. Society of Petroleum Engineers, 8-10 November 2010. Atyrau, Kazakhstan, SPE 139463-MS.

Allen, J.R., Wiggins, W.D., 1993. Dolomite reservoirs-geochemical techniques for evaluating origin and distribution. American Association of Petroleum Geologists, Continuing Education Course Notes, 36.

Alsharhan, A.S., Salah, M.G., 1997. Lithostratigraphy, sedimentology and hydrocarbon habitat of the Pre-Cenomanian Nubian sandstone in the Gulf of Suez Oil Province, Egypt. GeoArabia, 2 (4), 385-400.

Amthor, J.E., Mountjoy, E.W., Machel, H.G., 1993. Subsurface dolomites in Upper Devonian Leduc Formation buildups, central part of Rimbey-Meadowbrook Reef trend, Alberta, Canada. Bulletin of Canadian Petroleum Geology 41, 164-185.

Amthor, J.E., Mountjoy, E.W., Machel, H.G., 1994. Regional-scale porosity and permeability variations in Upper Devonian Leduc buildups: implications for reservoir development and prediction in carbonates. AAPG Bulletin 78, 1541-1559.

Bai, T., Pollard, D.D., Gao, H., 2000. Explanation for fracture spacing in layered materials. Nature 403, 753-756.

Bai, T., Maerten, L., Gross, M.R., Aydin, A., 2002. Orthogonal cross joints: do they imply a regional stress rotation? Journal of Structural Geology 24, 77-88.

Beliveau, D., Payne, D.A., Mundry, M., 1993. Waterflood and CO2 flood of the fractured Midale Field. Journal of Petroleum Technology 45 (9), 881-817.

Blatt, H., Middleton, G., Murray, R., 1972. Origin of sedimentary rocks. Prentice-Hall, Englewood Cliffs, NJ.

Bosworth, W., 1995. A high-strain rift model for the southern Gulf of Suez (Egypt). In: Lambiase, J.J., (Ed.), Hydrocarbon habitat in rift basins. Geological Society (London) Special Paper 80, 75–112

Bosworth W., Huchon P. & Mcclay K. 2005. The Red Sea and Gulf of Aden Basins. Journal of African Earth Sciences 43, 334-378.

Choquette, P.W., Pray, L.C., 1970. Geologic nomenclature and classification of porosity in sedimentary carbonates. AAPG Bulletin 54, 207-244.

Cochran, J.R., 1983. A model for the development of the Red Sea. AAPG Bulletin 67, 41-69.

Corbet, K., Friedman, M., Spang, J., 1987. Fracture development and mechanical stratigraphy of Austin Chalk, Texas. AAPG Bulletin 71, 17-28.

Dati, F., Guerriero, V., Iannace, A., Mazzoli, S., Vitale, S., Giorgioni, M., 2011. Fracture density as a function of crystal size: insights from a carbonate reservoir analogue. AAPG International Conference and Exhibition, Milan, Italy, October 23-26, 2011.

Dati, F., 2013. Characterization of a fractured carbonate reservoir analogue in the southern Apennines. Ph.D. thesis, Università Di Napoli "Federico II".

Di Naccio, D., Boncio, P., Cirilli, S., Casaglia, F., Morettini, E., Lavecchia, G., Brozzetti, F., 2005. Role of mechanical stratigraphy on fracture development in carbonate reservoirs: insights from outcropping shallow water carbonates in the Umbria–Marche Apennines, Italy. Journal of Volcanology and Geothermal Research 148 (1–2), 98-115.

Ehrenberg, S.N., Walderhaug, O., Bjørlykke, K., 2012. Carbonate porosity creation by mesogenetic dissolution: Reality or illusion? AAPG Bulletin 96 (2), 217-233.

El-Fiky, G., 2005. GPS-derived velocity and crustal strain field in the Suez-Sinai area, Egypt. Bulletin of the Earthquake Research Institute of the University of Tokyo 80, 73-86.

Flugel, E., 2010. Microfacies of Carbonate Rocks. Analysis, Interpretation and Application. 2nd Ed., XXIII, Pp. 984.

Gale, J.F.W., Laubach, S.E., Marrett, R.A., Olson, J.E., Holder, J., Reed, R.M., 2004. Predicting and characterizing fractures in dolostone reservoirs: using the link between diagenesis and fracturing. In: C. J. R. Braithwaite, G. Rizzi, and G. Darke (Eds.), The geometry and petrogenesis of dolomite hydrocarbon reservoirs: Geological Society (London) Special Publication 235, 177 – 192.Gawthorpe, R.L., Jackson, C.A.L., Young, M.J., Sharp, I.R., Moustafa, A.R., Leppard, C.W., 2003. Normal fault growth, displacement localisation and the evolution of normal fault populations: The Hammam Faraun Fault Block, Suez Rift, Egypt. Journal of Structural Geology 25(6), 883-895.

Giorgioni, M., Iannace, A., D'Amore, M., Dati, F., Galluccio, L., Guerriero, V., Mazzoli, S., Parente, M., Strauss, C., Vitale, S., 2016. Impact of early dolomitization on multi-scale petrophysical heterogeneties and fracture intensity of low-porosity platform carbonates (Albian-Cenomanian, Southern Apennines, Italy). Marine and Petroleum Geology 73, 462-478.

Gupta, S., Underhill, J.R., Sharp, I.R., Gawthorpe, R.L., 1999. Role of fault interactions in controlling synrift sediment dispersal patterns: Miocene, Abu Alaqa Group, Suez Rift, Sinai, Egypt. Basin Research 11, 167-189.

Halley, R.B., Scnmoker, J.W., 1983. High-Porosity Cenozoic Carbonate Rocks of South Florida: progressive loss of porosity with depth. AAPG Bulletin 67, 191-200.

Hirani, J., 2014. Integrated Structural, Sedimentological and Diagenetic Evaluation of Fault-Fracture controlled dolomite, Hammam Faraun Fault Block, Gulf of Suez. Ph.D. thesis, University of Manchester.

Hollis, C., Bastesen, E., Boyce, A., Corlett, H., Gawthorpe, R., Hirani, J., Rotevatn, A., Whitaker, F., 2017. Fault-controlled dolomitization in a rift basin. Geology, DOI:10.1130/G38394.1.

Jackson, C.A.L., Gawthorpe, R.L., Carr, I.D., Sharp, I.R., 2005. Normal faulting as a control on the stratigraphic development of shallow marine syn- rift sequences: the Nukhul and Lower Rudeis Formations, Hammam Faraun Fault Block, Suez Rift, Egypt. Sedimentology 52, 313-338.

Jackson, C.A.L., Gawthorpe, R.L., Leppard, C.W., Sharp, I.R., 2006. Rift-initiation development of normal fault blocks: insights from the Hammam Faraun Fault Block, Suez Rift, Egypt. Journal of the Geological Society 163 (1), 165-183.

Jackson & Rotevatn, 2013)

Khalil, S.M., McClay, K.R., 2001. Tectonic evolution of the NW Red Sea-Gulf of Suez Rift System. Geological Society of London Special Publications 187(1), 453-473.

Laubach, S. E., Olson, J. E, and Gross, M. R., 2009, Mechanical and fracture stratigraphy. AAPG Bulletin, v. 93, no. 11, p. 1413-1426.

Lezin, C., Odonn, F., Massonat, G.J., Escadeillas, G., 2009. Dependence of joint spacing on rock properties in carbonate strata. AAPG Bulletin 93, 271-290.

Lucia, F.J., Major, R.P., 1994. Porosity evolution through hypersaline reflux dolomitization. In: Purser, B.H., Tucker, M.E. & Zenger, D.H. (Eds.), Dolomites: A volume in honour of dolomieu. International Association of Sedimentologists, Special Publications 21, 325-341.

Lucia, F.J., 2002. Origin and petrophysics of dolostone pore space. In: Rtzzl, G., Darke, G. & Braithwaite, C.J.R. (Eds.), The Geometry and petrogenesis of dolomite hydrocarbon reservoirs. Final programme and abstracts. Geological Society Petroleum Group, London.

Lucia, F.J., 2004. Origin and petrophysics of dolostones pore space. In: Braithwaite, C.J.R., Rizzi, G., Darke, G. (Eds.), The geometry and petrogenesis of dolomite hydrocarbon reservoirs: Geological Society of London Special Publications 235, 7-63.

Machel, H.G., 2004. Concepts and models of dolomitization: A critical reappraisal. In: Braithwaite, C.J.R., Rizzi, G., Darke, G. (Eds.), The geometry and petrogenesis of dolomite hydrocarbon reservoirs: Geological Society of London Special Publications 235, 7-63.

Moustafa, A.R., 1996. Internal structure and deformation of an accommodation zone in the northern part of the Suez Rift. Journal of Structural Geology 18, 93–107.

Moustafa, A.R., 2004. Geologic maps of the eastern side of the Suez Rift (western Sinai Peninsula), Egypt. AAPG Datapages, Inc. GIS Series (Geologic maps and cross-sections in digital format on CD).

Moustafa, A.R., Abdeen, A.R., 1992. Structural setting of the Hammam Faraun Block, Eastern Side of The Suez Rift. Journal of the University of Kuwait (Science) 19, 291–310.

Nelson, R.A., 2001. Geologic Analysis of Fractured Reservoirs: Second Edition, 352 p.

Nelson, R.A., 2015, Characterization and Evaluation of Natural Fracture Effects in Carbonate and Vuggy Carbonate Reservoirs and How it Differs from Other Fractured Reservoirs; abst. 1st Mountjoy Conf. Advances in Characterization and Modeling of Complex Carbonate Reservoirs, Banff, Aug. 23-28, 2015.

Ortega, O., Marrett, R., 2001. Stratigraphic controls on fracture intensity in Barremian-Aptian carbonates, northeastern Mexico: in Marrett, R., (Eds.), Genesis and controls of reservoir-scale carbonate deformation, Monterrey salient, Mexico: Austin, Texas, Bureau of Economic Geology, Guidebook 28, p. 57-82.

Ortega, O.J., Marrett, R.A., Laubach, S.E., 2006. A scale-independent approach to fracture intensity and average spacing measurement. AAPG Bulletin 90 (2), 193-208.

Patton, T.L., Moustafa, A.R., Nelson, R.A., Abdine, S.A., 1994. Tectonic evolution and structural setting of the Suez Rift. In: S.M. Landon (ed.), Interior rift basins. AAPG Memoir 59, 7-55.

Purser, B., Tucker, M., Zenger, D., 1994. Dolomites: A Volume In Honor Of Dolomieu. International Association of Sedimentologists Special Publication 21, 325-341.

Rustichelli, A., Agosta, F., Tondi, E., Spina, V., 2013. Spacing and distribution of bed-perpendicular joints throughout layered, shallow-marine carbonates (Granada Basin, Southern Spain). Tectonophysics 582, 188-204.

Rustichelli, A., Iannace, A., Girundo, M., 2015. Dolomitization impact on fracture density in pelagic carbonates: contrasting case studies from the Gargano Promontory and the southern Apennines (Italy). Italian Journal of Geosciences 134 (3), 556-575.

Saller, A.H., Henderson N., 2001. Distribution of porosity and permeability in platform dolomites: insight from the Permian of West Texas: reply. AAPG Bulletin 85, 530-532.

Saller, A.H. 2013. Diagenetic Evolution of Porosity in Carbonates during Burial. Adapted from AAPG Distinguished Lecture and main part of presentation at Tulsa Geological Society Luncheon Meeting, January 15, 2013.

Schmoker, J.W., Halley, R.B., 1982. Carbonate porosity versus depth: a predictable relationfor south Florida. AAPG Bulletin 66, 2561-2570.

Schmoker, J.W., Krystinik, K.B., Halley, R.B., 1985. Selected characteristics of limestone and dolomite reservoirs in the United States. AAPG Bulletin 69(5), 733-741.

Sharp, I.R., Gawthorpe, R.L., Underhill, J.R., Gupta, S., 2000. Fault-propagation folding in extensional settings: examples of structural style and synrift sedimentary response from the Suez rift, Sinai, Egypt. Geological Society of America Bulletin 112, (12) 1877-1899.

Sibley, D., Gregg, J., 1987. Classification of dolomite rock textures. J. of Sed. Petr. 57, 967-975.

Spence, G.H., Finch, E., 2014. Influences of nodular chert rhythmites on natural fracture networks in carbonates: an outcrop and two-dimensional discrete element modelling study. In: Spence G. H., Redfern J., Aguilera R.,Bevan T. G., Cosgrove J. W., Couples G. D., Daniel J.-M. (Eds.), Advances in the Study of Fractured Reservoirs, Geological Society of London Special Publications.

Sun, S.Q., 1995. Dolomite Reservoirs: Porosity Evolution and Reservoir Characteristics. AAPG Bulletin 79, 186-204.

Wennberg, O.P., Svånå, T., Azizzadeh, M., Aqrawi, A.M.M., Brockbank, P., Lyslo, K.B., Ogilvie, S., 2006. Fracture intensity vs. mechanical stratigraphy in platform top carbonates: the aquitanian of the Asmari Formation, Khaviz Anticline, Zagros, SW Iran. Petroleum Geoscience 12(3), 235-246.

Younes, A.I., McClay, K., 2002. Development of accommodation zones in the Gulf of Suez-Red Sea rift, Egypt. AAPG Bulletin 86, (6) 1003-1026.

Zahm, C.K., Zahm, L.C., Bellian, J.A., 2010. Integrated fracture prediction using sequence stratigraphy within a carbonate fault damage zone, Texas, USA. Journal of Structural Geology 32(9), 1363-1374.

Figures captions:

Fig. 1. A. Regional structural map of the Suez Rift (adapted from Alsharhan and Salah (1997) and Younes and McClay (2002)). The bold line marks the location of the regional cross-section shown in D. B. Geological map of the study area located at the footwall of the Hammam Faraun Fault. Two areas of particular focus in this study area are marked with orange stars. One of these areas is located in the immediate vicinity of the HFF, whereas the other is located approximately 2 km into the HFF footwall. C. Stratigraphic column of the succession in the study area and surrounding regions (adapted from Sharp et al., 2000; Jackson et al., 2006). Violet color within the Thebes Fm. indicates dolostones. D. Regional cross-section across the Gulf of Suez showing the rift structure (Sharp et al., 2000); location is shown in A.

Fig. 2. A. Burial curve of the Thebes Fm. showing the timing of two phases of dolostone formation (stratabound and massive dolostones) (Hirani, 2014). B-C. Outcrop photographs illustrating the structural position of dolostones.

Fig. 3. A. Conglomerate (undolomitized) displaying packstone texture of clast and wackestone texture of matrix. B-C. Grainstone (undolomitized) composed of bioclasts and intragranular, mouldic and vuggy pores. D. Highly cemented packstone (undolomitized) with intergranular and vuggy pores.

Fig. 4. Quantitative modal analysis of textures in limestone (A), massive dolostone (B) and stratabound dolostone (C) showing average area occupied by grains, matrix, pores and cement in the whole rock. Average area of different pore types in limestone (D), massive dolostone (E) and stratabound dolostone (F). Note that in all the histograms data are shown by lithofaces as defined in the legend.

Fig. 5. Grain/crystal size (A), pore size (B), porosity (C) and Young's modulus (D) of the studied limestone and dolostone lithofacies. Note that all the data are shown by lithofaces as defined in the legend. The box represents the mean, whereas the extent of the bars shows the 90% of values. Violet dotted lines mark the average value for limestone, massive dolostone and stratabound dolostone.

Fig. 6. Conglomerate (massive dolostone) partially preserved primary textures of precursor limestone (A, B). Packstone (massive dolostone) displaying intercrystalline and vuggy pores (C, D).

Fig. 7. Fracture distribution within undolomitized conglomerate c. 2 km from the HFF (A), massively dolomitized conglomerate (D) close to the HFF and undolomitized packstone (B) and massively dolomitized packstone (B-D). Note that thin reddish intercalated beds (indicated by arrows) within both packstone (B) and dolomitized packstone (C), act as mechanical interfaces for stratabound joints.

Fig. 8. Rose diagrams showing the orientations of fractures at 2 km (A) and 100 m (B) distance from the HFF. Cross-plot of fracture intensity vs. bed thickness for the studied rocks at 2 km distance from the HFF (C) and at 100 m distance from the HFF (D). Note a positive linear relationship between fracture intensity and bed thickness shown in both (C) and (D). Histogram shows average spacing, normalized to bed thickness, for undolomitized and dolomitized lithofacies at distance (2 km) from the fault (E) and near (100 m) the fault (F).

Fig. 9. The average values of porosity (A), pore size (B), grain/crystal size (C) and fracture spacing within limestones and dolostones at 2 km distance from the HFF (D) and in the vicinity (100 m) of the HFF (E).

Table caption:

Table 1. Lithological, textural and petrophysical characteristics of conglomerate, grainstone, packstone and their stratabound and massive dolomitized equivalents.

Table 2. Fracture spacing within different lithologies (either undolomitized or dolomitized) at 100 m and 2 km distance from the HFF

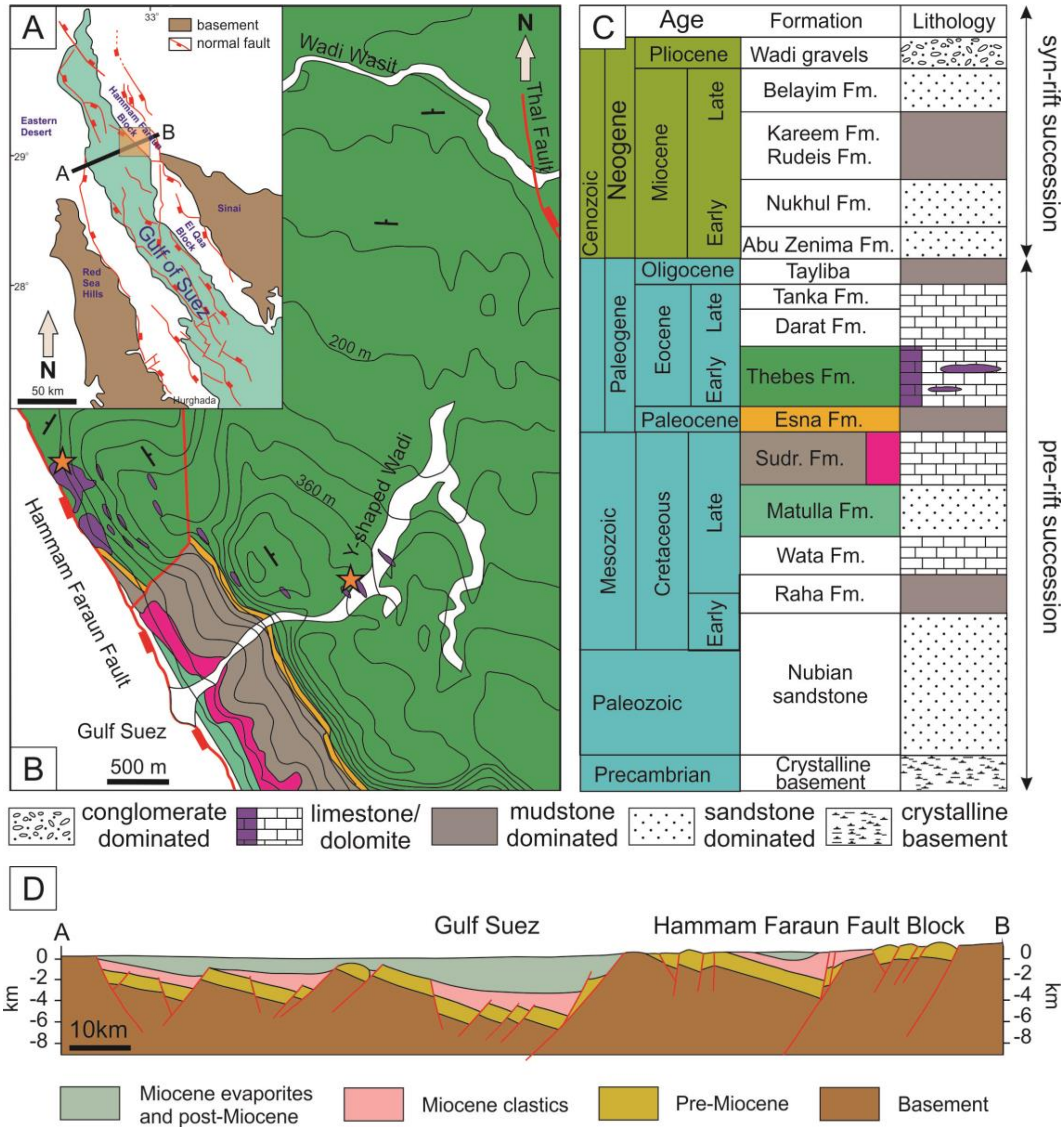

Figure 1A. Regional structural map of the Suez Rift (adapted from Alsharhan and Salah (1997) and Younes and McClay (2002)). The bold line marks the location of the regional crosssection shown in D. B. Geological map of the study area located at the footwall of the Hammam Faraun Fault. Two areas of particular focus in this study area are marked with orange stars. One of these areas is located in the immediate vicinity of the HFF, whereas the other is located approximately 2 km into the HFF footwall. C. Stratigraphic column of the succession in the study area and surrounding regions (adapted from Sharp et al., 2000; Jackson et al., 2006). Violet color within the Thebes Fm. indicates dolostones. D. Regional cross-section across the Gulf of Suez showing the rift structure (Sharp et al., 2000); location is shown in A. (For interpretation of the references to colour in this figure legend, the reader is referred to the web version of this article.)

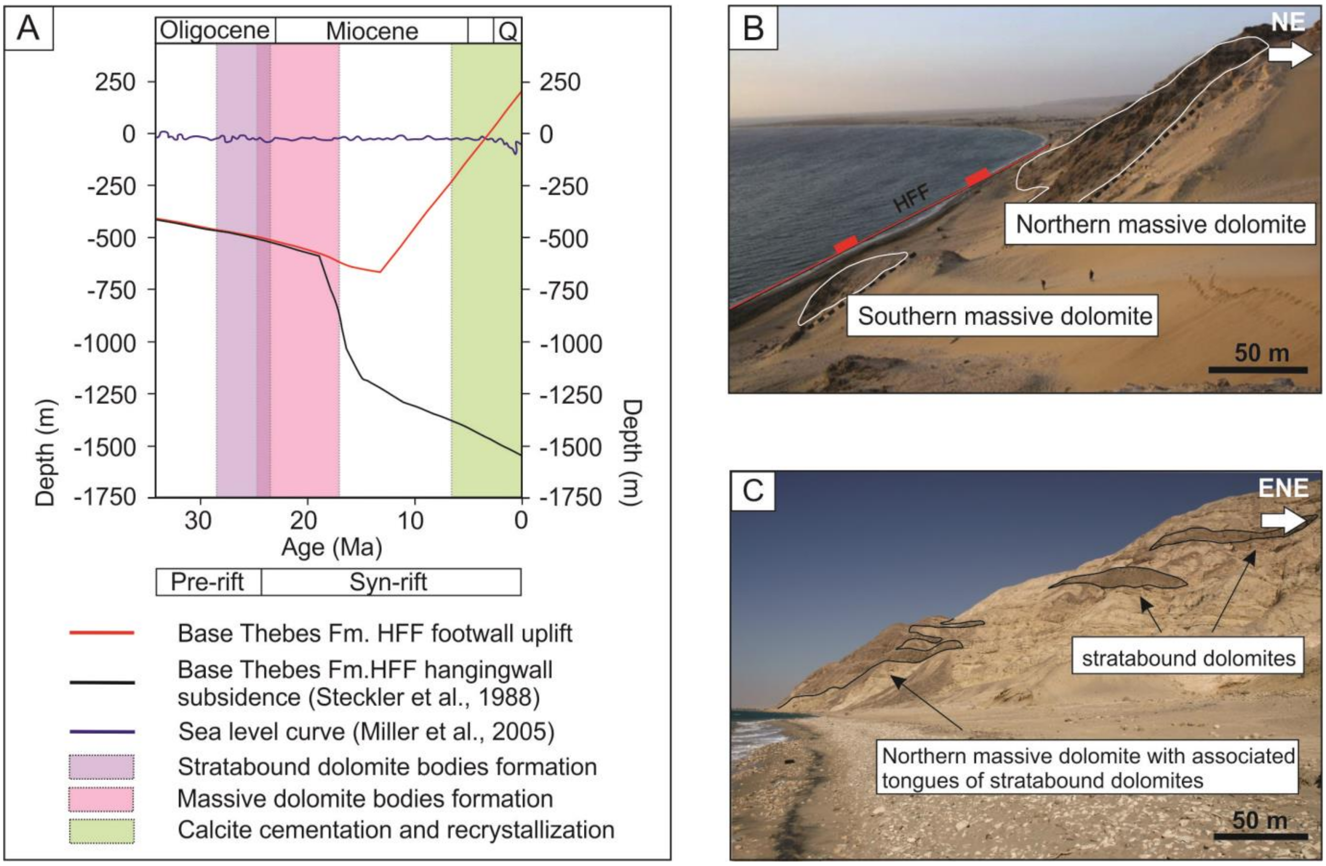

Figure 2 A. Burial curve of the Thebes Fm. showing the timing of two phases of dolostone formation (stratabound and massive dolostones) (Hirani, 2014). BeC. Outcrop photographsillustrating the structural position of dolostones.

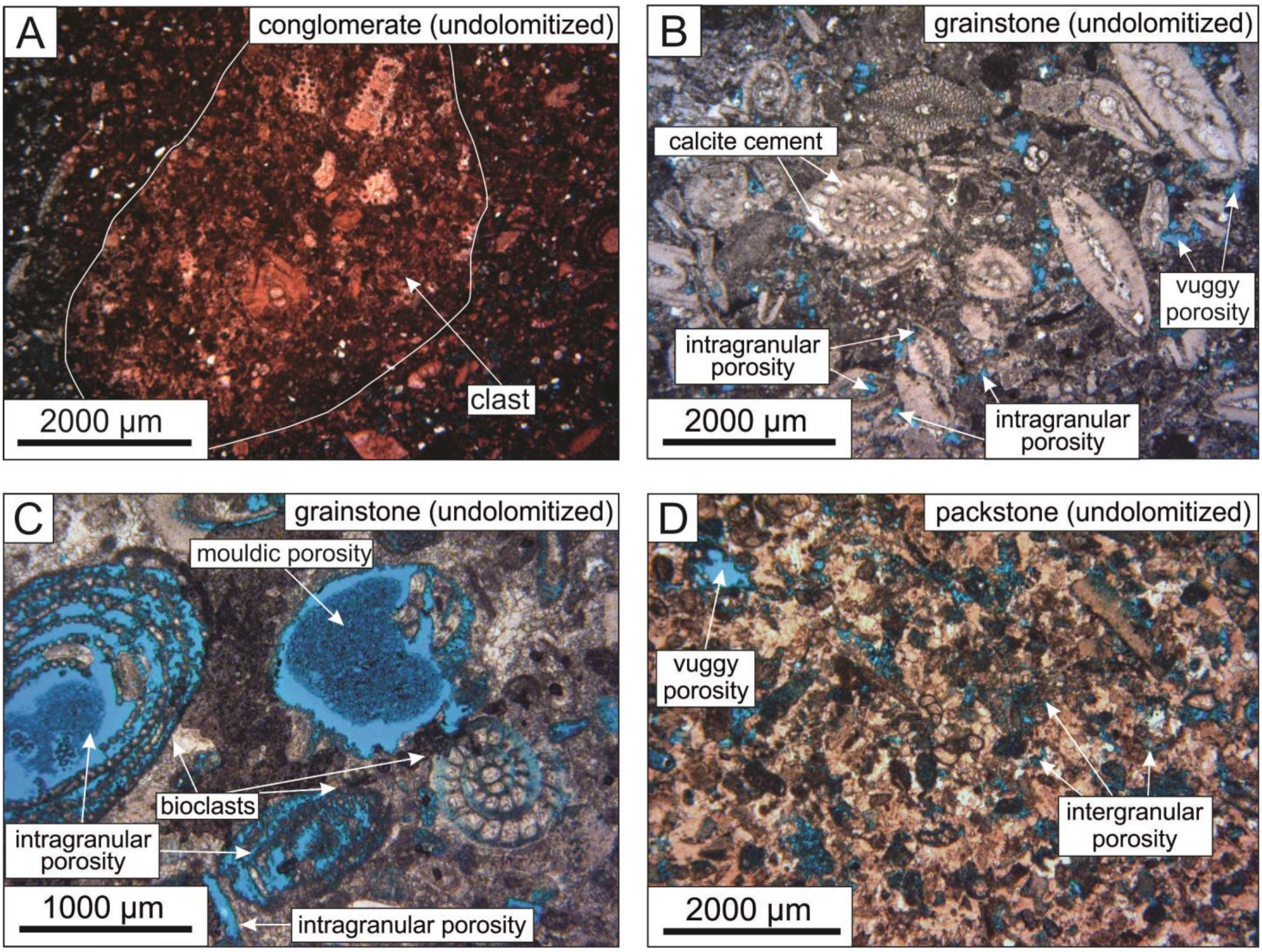

Figure 3A. Conglomerate (undolomitized) displaying packstone texture of clast and wackestone texture of matrix. BeC. Grainstone (undolomitized) composed of bioclasts and intragranular, mouldic and vuggy pores. D. Highly cemented packstone (undolomitized) with intergranular and vuggy pores.

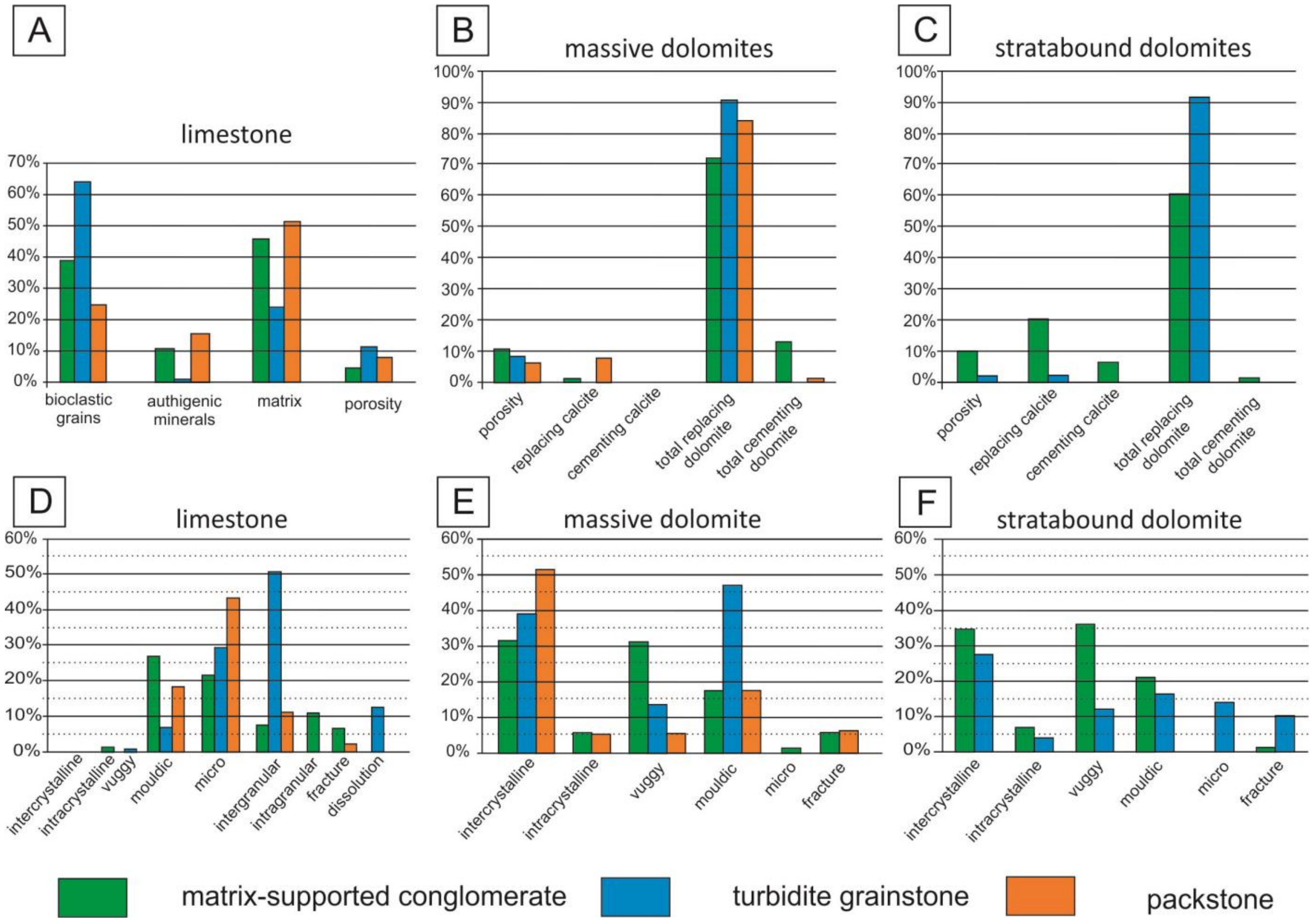

Figure 4 Quantitative modal analysis of textures in limestone (A), massive dolostone (B) and stratabound dolostone (C) showing average area occupied by grains, matrix, pores and cement in the whole rock. Average area of different pore types in limestone (D), massive dolostone (E) and stratabound dolostone (F). Note that in all the histograms data are shown by lithofaces as defined in the legend.

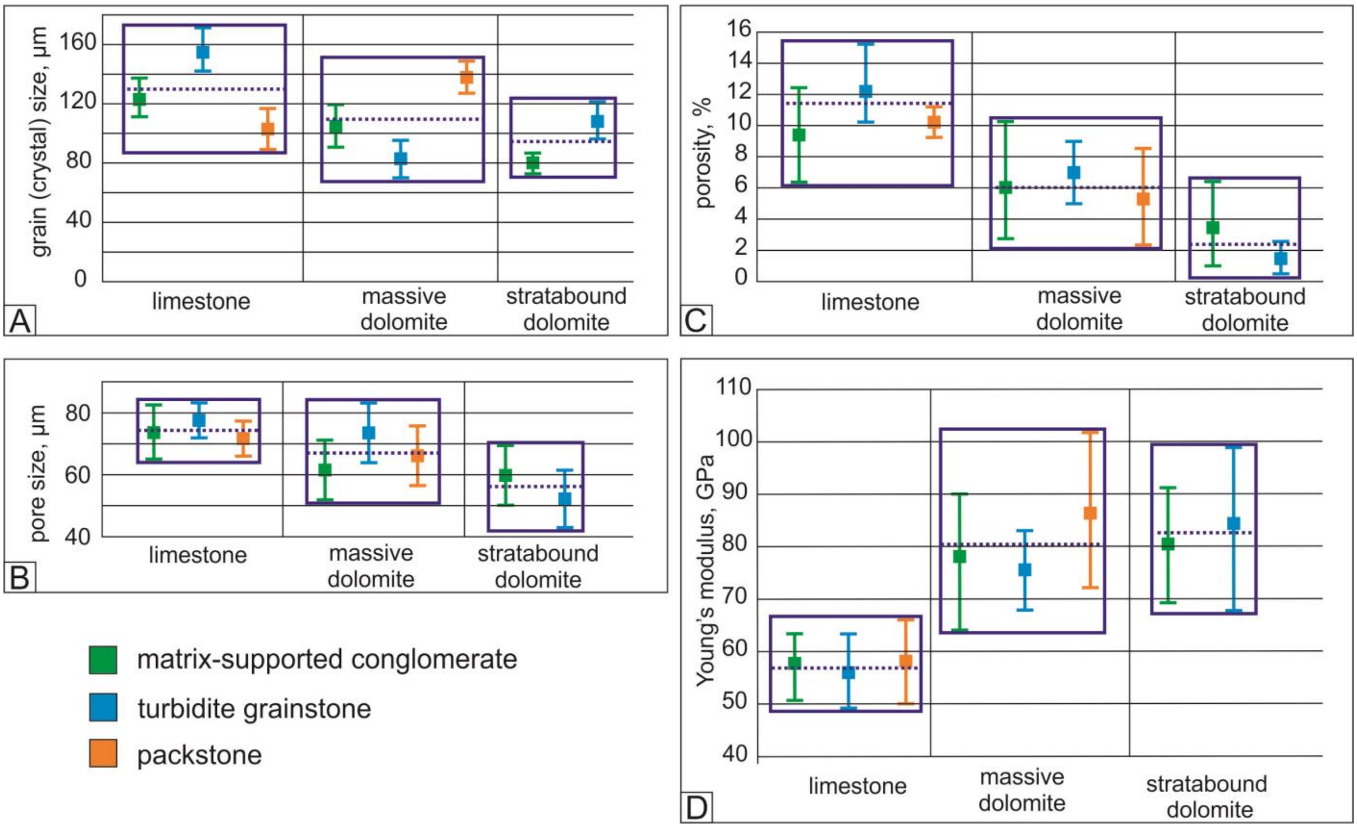

Figure 5 Grain/crystal size (A), pore size (B), porosity (C) and Young's modulus (D) of the studied limestone and dolostone lithofacies. Note that all the data are shown by lithofaces as defined in the legend. The box represents the mean, whereas the extent of the bars shows the 90% of values. Violet dotted lines mark the average value for limestone, massive dolostone and stratabound dolostone. (For interpretation of the references to colour in this figure legend, the reader is referred to the web version of this article.)

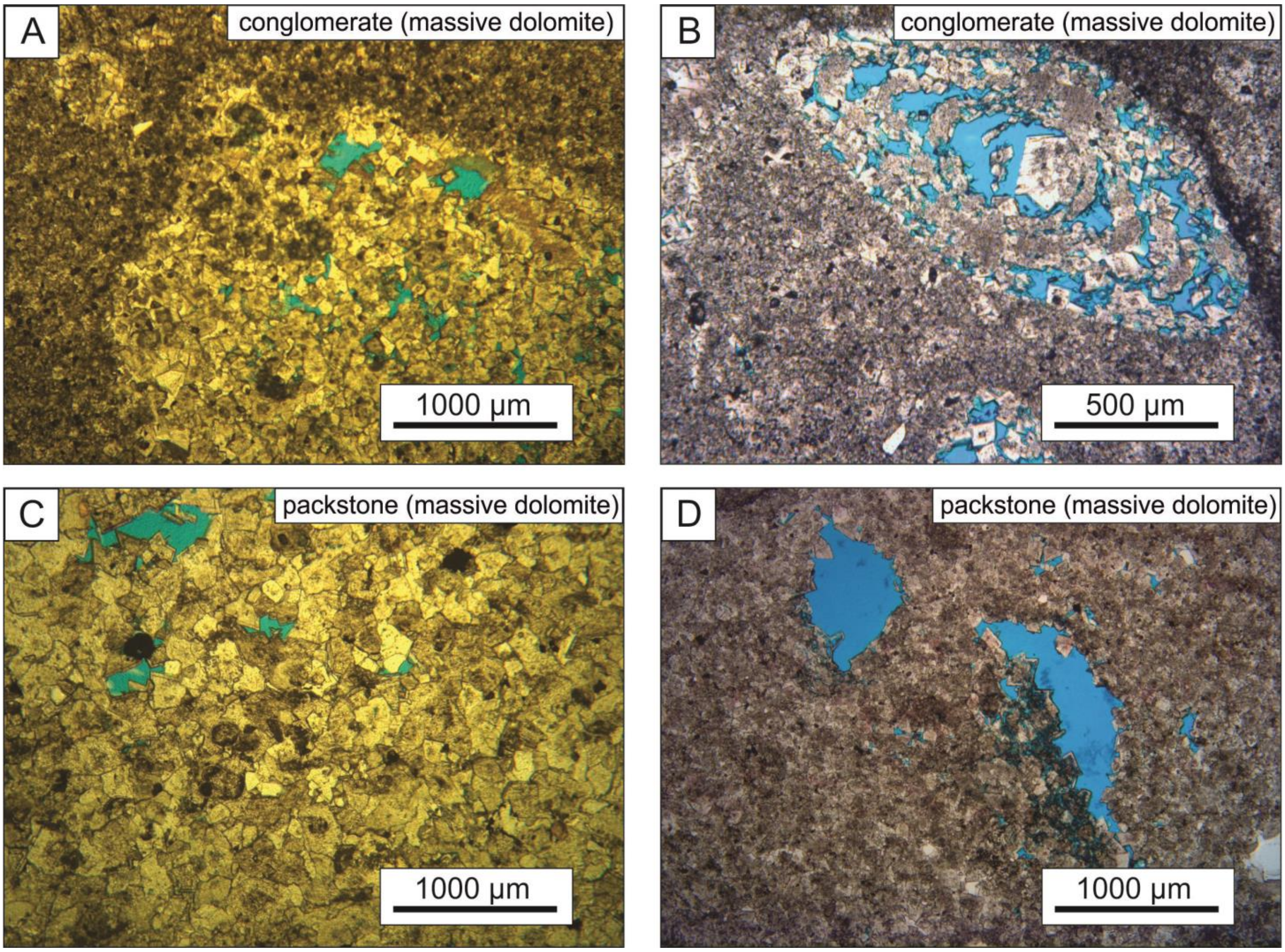

Figure 6 Conglomerate (massive dolostone) partially preserved primary textures of precursor limestone (A, B). Packstone (massive dolostone) displaying intercrystalline and vuggy pores (C, D).

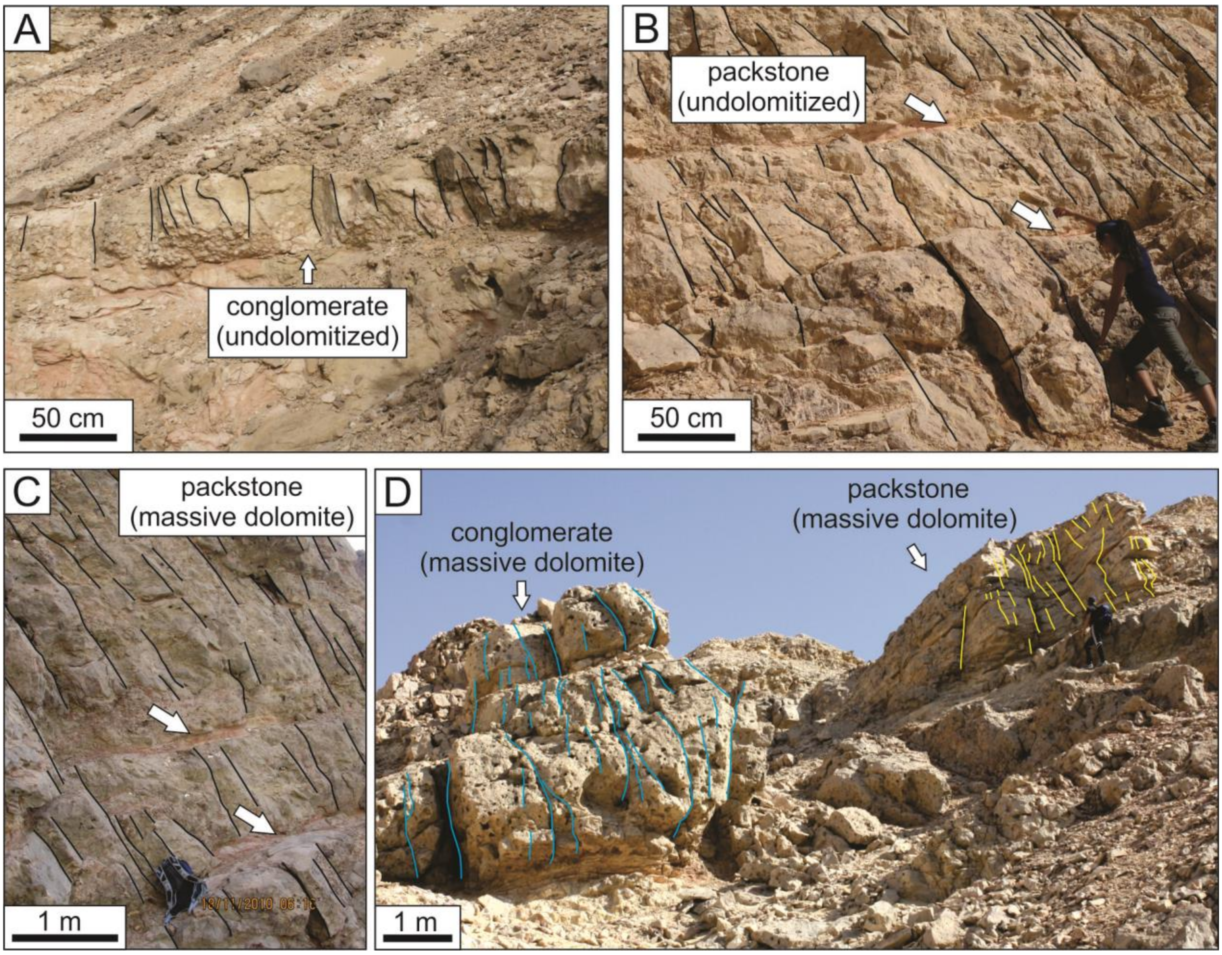

Figure 7 Fracture distribution within undolomitized conglomerate c. 2 km from the HFF (A), massively dolomitized conglomerate (D) close to the HFF and undolomitized packstone (B) and massively dolomitized packstone (BeD). Note that thin reddish intercalated beds (indicated by arrows) within both packstone (B) and dolomitized packstone (C), act as mechanical interfaces for stratabound joints. (For interpretation of the references to colour in this figure legend, the reader is referred to the web version of this article.)

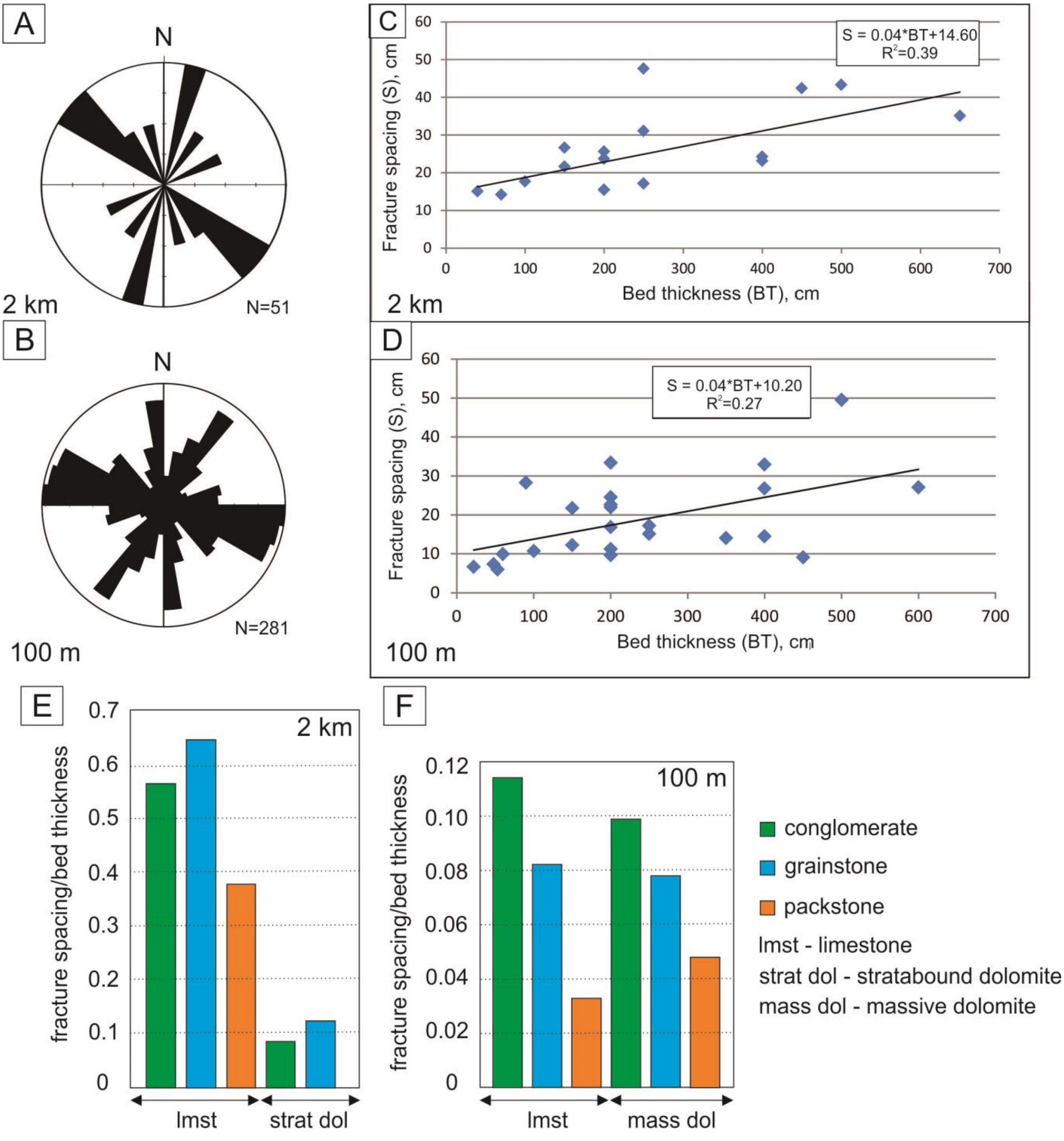

Figure 8 Rose diagrams showing the orientations of fractures at 2 km (A) and 100 m (B) distance from the HFF. Cross-plot of fracture intensity vs. bed thickness for the studied rocks at 2 km distance from the HFF (C) and at 100 m distance from the HFF (D). Note a positive linear relationship between fracture intensity and bed thickness shown in both (C) and (D). Histogram shows average spacing, normalized to bed thickness, for undolomitized and dolomitized lithofacies at distance (2 km) from the fault (E) and near (100 m) the fault (F).

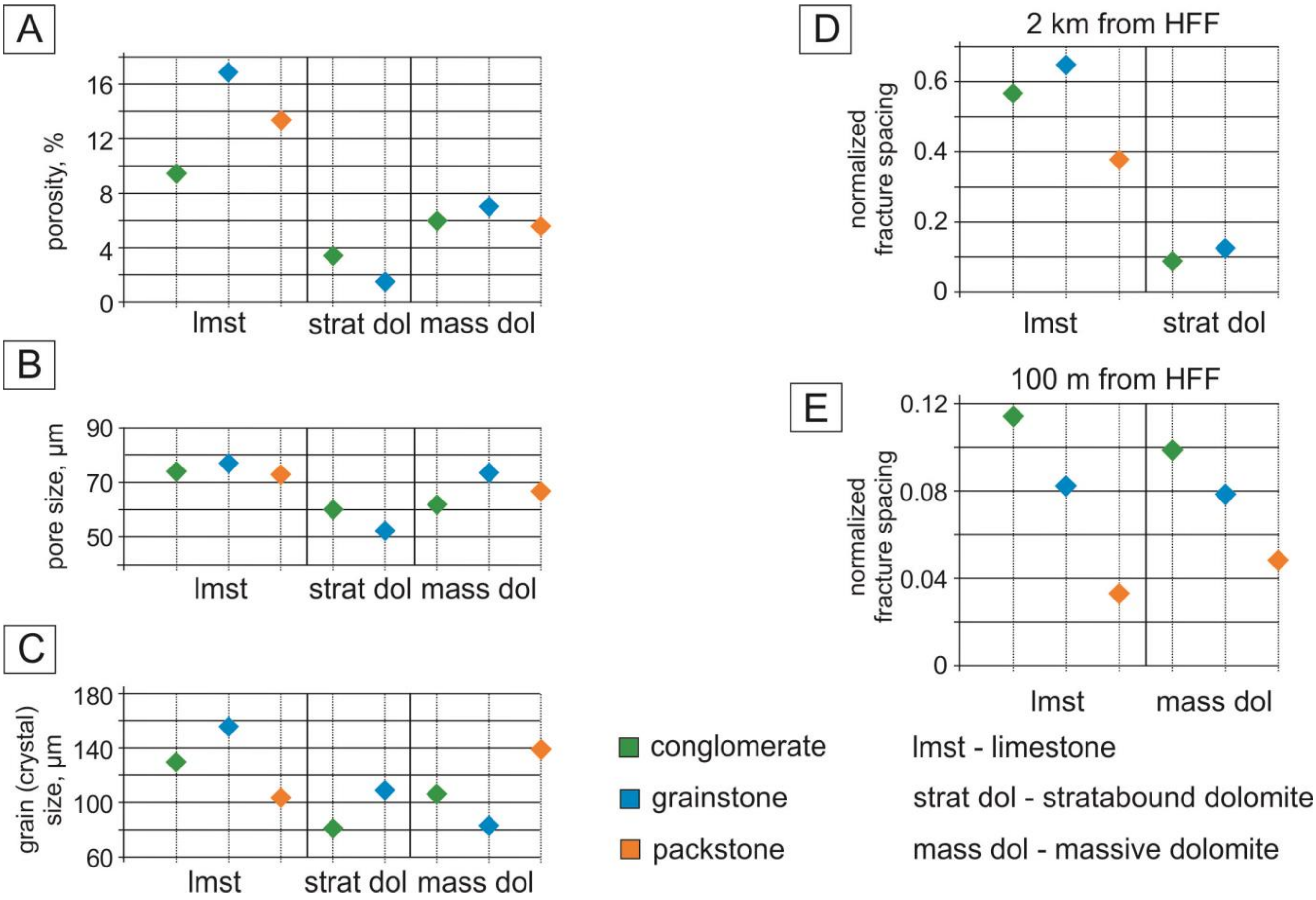

Figure 9 The average values of porosity (A), pore size (B), grain/crystal size (C) and fracture spacing within limestones and dolostones at 2 km distance from the HFF (D) and in the vicinity (100 m) of the HFF (E).

			Bed thickness (cm)	Average grain size (um)	Total (helium) porosity (%)	Pore size (um)	Dominant pore type	Young modulus (GPa)	Permeability (mD)
Undolomitized	conglomerate	average	**172**	**120**	**9**	**73**	micro, moldic	**58**	**0.35**
		min	50	20	6	65		50	0.003
		max	300	435	13	85		63	1.51
	grainstone	average	**234**	**156**	**12**	**77**	intergranular, micro	**56**	**0.42**
		min	40	70	10	55		49	0.1
		max	450	425	16	93		63	2.20
	packstone	average	**153**	**100**	**10**	**72**	micropores, mouldic, intergranular	**58**	**0.10**
		min	22	88	9	67		50	0.03
		max	600	108	11	77		67	1.51
Massive dolomite	conglomerate	average	**250**	**108**	**6**	**60**	Intercrystalline, vuggy, moldic	**78**	**0.51**
		min	50	90	3	50		63	0.003
		max	600	120	10	71		90	2.30
	grainstone	Average	**278**	**81**	**7**	**73**	Intercrystalline, moldic, vuggy	**75**	**0.06**
		min	100	69	5	65		68	0.008
		max	800	96	9	85		82	0.21
	packstone	average	**130**	**139**	**6**	**67**	Intercrystalline, moldic	**87**	**0.57**
		min	90	128	2	56		72	0.003
		max	200	150	8	76		102	1.65
Stratabound dolomite	conglomerate	average	**467**	**81**	4	**60**	intercrystalline, vuggy, moldic	**80**	**0.12**
		min	400	20	1	50		70	0.003
		max	500	285	7	70		91	0.6
	grainstone	average	**275**	**108**	**2**	**52**	intercrystalline, moldic, vuggy, micro, fracture	**84**	**0.20**
		min	250	95	3	42		68	0.004
		max	300	122	1	61		100	0.56

Table 1 Lithological, textural and petrphysical characteristics of conglomerate, grainstone, packtone and their stratabound and massive dolomitzed equivalents

			Standard deviation	Mean spacing	Cv	Normalized average spacing
2 km from the HFF	Undolomitized	conglomerate	3.69	19.96	0.19	0.57
		grainstone	3.22	30.41	0.11	0.65
		packstone	6.12	22.00	0.28	0.38
	Stratabound dolomite	conglomerate	11.27	47.62	0.24	0.09
		grainstone	7.13	20.91	0.34	0.12
100 m from the HFF	Undolomitized	conglomerate	7.93	21.12	0.38	0.11
		grainstone	10.01	21.45	0.47	0.08
		packstone	10.23	11.69	0.88	0.03
	Massive dolomite	conglomerate	17.45	29.60	0.59	0.10
		grainstone	9.31	18.80	0.50	0.07
		packstone	1.12	9.03	0.12	0.05

Table 2 Fracture spacing within different lithologies (either undolomitized or dolomitized) at 100 m and 2 km distance from the HFF.